HHS Public Access

Author manuscript

Exp Eye Res. Author manuscript; available in PMC 2023 December 01.

Published in final edited form as:

Exp Eye Res. 2022 December ; 225: 109279. doi:10.1016/j.exer.2022.109279.

Synaptotagmins 1 and 7 in vesicle release from rods of mouse retina

C.S. Mesnard[a,b,1], **C.L. Hays**[a,1], **C.L. Barta**[a], **A.L. Sladek**[a], **J.J. Grassmeyer**[a,b], **K.K. Hinz**[a], **R.M. Quadros**[b,c], **C.B. Gurumurthy**[b,c], **W.B. Thoreson**[a,b,*]

[a]Truhlsen Eye Institute and Department of Ophthalmology and Visual Sciences, USA

[b]Pharmacology and Experimental Neuroscience, USA

[c]Mouse Genome Engineering Core Facility, Vice Chancellor for Research Office, College of Medicine, University of Nebraska Medical Center, Omaha, NE, 68106, USA

Abstract

Synaptotagmins are the primary Ca^{2+} sensors for synaptic exocytosis. Previous work suggested synaptotagmin-1 (Syt1) mediates evoked vesicle release from cone photoreceptor cells in the vertebrate retina whereas release from rods may involve another sensor in addition to Syt1. We found immunohistochemical evidence for syntaptotagmin-7 (Syt7) in mouse rod terminals and so performed electroretinograms (ERG) and single-cell recordings using mice in which Syt1 and/or Syt7 were conditionally removed from rods and/or cones. Synaptic release was measured in mouse rods by recording presynaptic anion currents activated during glutamate re-uptake and from exocytotic membrane capacitance changes. Deleting Syt1 from rods reduced glutamate release evoked by short depolarizing steps but not long steps whereas deleting Syt7 from rods reduced release evoked by long but not short steps. Deleting both sensors completely abolished depolarization-evoked release from rods. Effects of various intracellular Ca^{2+} buffers showed that Syt1-mediated release from rods involves vesicles close to ribbon-associated Ca^{2+} channels whereas Syt7-mediated release evoked by longer steps involves more distant release sites. Spontaneous release from rods was unaffected by eliminating Syt7. While whole animal knockout of Syt7 slightly reduced ERG b-waves and oscillatory potentials, selective elimination of Syt7 from rods had no effect on ERGs. Furthermore, eliminating Syt1 from rods and cones abolished ERG b-waves and additional elimination of Syt7 had no further effect. These results show that while Syt7 contributes to slow non-ribbon release from rods, Syt1 is the principal sensor shaping rod and cone inputs to bipolar cells in response to light flashes.

Keywords

Rods; Cones; Electroretinogram; Exocytosis; Mouse; Neuroscience; Retina; Ribbon synapse

[*]Corresponding author. Truhlsen Eye Institute and Department of Ophthalmology and Visual Sciences University of Nebraska Medical Center S 45th St, Omaha, NE, 68106, USA., wbthores@unmc.edu (W.B. Thoreson).

[1]Both authors contributed equally.

Appendix A. Supplementary data

Supplementary data to this article can be found online at https://doi.org/10.1016/j.exer.2022.109279.

1. Introduction

Light-evoked voltage changes generated in the outer segments of rod and cone photoreceptor cells are transmitted at their synapses to downstream neurons. Transmission across this first synapse in the retina thus determines what information collected by rods and cones is available to the visual system. Vesicle release from rods and cones involves plate-like protein structures known as synaptic ribbons. Ribbons are also present at sensory synapses of cochlear and vestibular hair cells as well as retinal bipolar cells (Moser et al., 2020; Thoreson, 2021). Voltage-gated Ca^{2+} channels cluster beneath these ribbons, ideally positioned for precise regulation of release (Nachman-Clewner et al., 1999; tom Dieck et al., 2005). Previous studies have shown that while release from cones appears to occur solely at synaptic ribbons, rods are capable of release at both ribbon and non-ribbon sites further away from Ca^{2+} channels (Chen et al., 2013, 2014). Non-ribbon release from rods involves Ca^{2+}-induced Ca^{2+} release (CICR) from intracellular stores and inhibiting CICR substantially reduced light responses of second-order neurons, including a 50% reduction in the ERG b-wave of mouse retina (Babai et al., 2010; Cadetti et al., 2006; Krizaj et al., 2003; Suryanarayanan and Slaughter, 2006). These results suggested that non-ribbon release from rods might play a significant role in encoding their light responses.

Genetic elimination of the Ca^{2+} sensor molecule, synaptotagmin-1 (Syt1), abolished release from mouse cones (Grassmeyer et al., 2019). However, while eliminating Syt1 abolished the release from rods evoked by short depolarizing steps, rods retained some ability for release when stimulated with 25 ms steps (Grassmeyer et al., 2019). We hypothesized that this slower component of release evoked by longer steps might be due to release from non-ribbon sites and use a different exocytic Ca^{2+} sensor. Syt7 shows a higher Ca^{2+} affinity than Syt1 and mediates a slow component release in retinal bipolar cells and other CNS neurons, making it a good candidate to mediate slow, non-ribbon release from rods (Bacaj et al., 2013; Luo et al., 2015; MacDougall et al., 2018; Turecek and Regehr, 2018).

To test the roles of Syt1 and Syt7 in regulating release from rods and cones, we created mouse lines that allowed selective elimination of these sensors from rods or cones (Quadros et al., 2017). To assess glutamate release from rods and cones, we used the electroretinogram (ERG), an extracellular field potential that arises from retinal activity, along with whole cell patch clamp recordings of membrane capacitance changes and anion currents generated during glutamate re-uptake into individual rods. Our results show that in mouse rods, Syt1 controls fast, synchronous glutamate release from ribbons whereas Syt7 contributes to slower release involving more distant sites stimulated by the spread of Ca^{2+} that accompanies lengthy depolarizing stimulation. However, in the absence of Syt1, Syt7 is unable to generate significant ERG b-waves. Thus, Syt1-mediated release appears to be entirely responsible for encoding light responses at both rod and cone synapses with little or no direct contribution from Syt7-mediated non-ribbon release. Instead, slow release at non-ribbon sites mediated by Syt7 may modulate synaptic activity by shaping cleft glutamate levels.

2. Materials and methods

2.1. Mice

Control C57Bl6J and mutant mice aged 4–8 weeks were used for these experiments. Creation of HRGP-Cre, Rho-iCre, and Syt1^{flox} (Syt1: MGI:99667) mice have been described previously (Le et al., 2004; Li et al., 2005; Quadros et al., 2017). Syt1$^{fl/fl}$ mice were originally created using C57Bl6N mice. Genetic screening showed that Syt1$^{fl/fl}$ mice used for these experiments were 40% C57/Bl6J. Additional details of Syt1^{flox} mice are described elsewhere (Quadros et al., 2017; Grassmeyer et al., 2019). Yun Le (Univ. of Oklahoma) generously provided HRGP-Cre mice. Rho-iCre mice were obtained from Jackson Laboratories, Bar Harbor, ME (B6.Cg-*Pde6b*$^{+}$ Tg(Rho-iCre)1Ck/Boc; RRID: 015850). Rho-iCre and HRGP-Cre mice selectively express cre-recombinase in rods and cones, respectively (Le et al., 2004; Li et al., 2005; Jin et al., 2020).

Syt7^{flox} and Syt7 knockout mice were created by the UNMC Mouse Genome Engineering Core, Nebraska Medical Center (Table 1). Syt7^{flox} mice were generated by introducing *LoxP* sites into C57Bl6J mice that flanked exon 5 of Syt7 transcript 201 (ENSMUSE0000022570) using *Easi*-CRISPR (Quadros et al., 2017). This exon was also deleted in Syt7 knockout mice used for ERG experiments. Further details on creation of Syt7^{flox} mice are described in the results. To eliminate Syt1 and Syt7 selectively from rods and cones, we crossed Rho-iCre and HRGP-Cre mouse lines with Syt1$^{fl/fl}$ and Syt7$^{fl/fl}$ mice. Most Cre-negative Syt1$^{fl/fl}$ and Syt7$^{fl/fl}$ mice were used for breeding and so most control experiments were done using wild type C57Bl6J mice.

Euthanasia was conducted in accordance with AVMA Guidelines for the Euthanasia of Animals by CO_2 asphyxiation followed by cervical dislocation. All animal care and handling protocols were approved by the University of Nebraska Medical Center Institutional Animal Care and Use Committee.

2.2. Electroretinography

ERGs were recorded in vivo using a UTAS Sunburst ganzfeld illuminator (LKC, Gaithersburg, MD, LKC-UTAS-SB). Mice were dark-adapted for ~12 h prior to experiments and then anaesthetized via intra-peritoneal injection with a ketamine/xylazine drug cocktail (100 mg/kg ketamine, 10 mg/kg xylazine). Core temperature of the mouse was maintained at 37 °C with a heat pad. Tropicamide and proparacaine ophthalmic solution (0.5%) were administered topically to the left eye before the mouse was secured to the platform and a silver/silver chloride wire ring recording electrode was centered on the left cornea. Subcutaneous ground and reference electrodes were placed at the base of the tail and under the scalp, respectively. ERG a-waves provide a measure of photoreceptor responses and were measured from baseline to the bottom of the inward going negative potential. ERG b-waves reflect responses of second-order ON-type bipolar cells and were measured from the trough of the initial negative deflection of the a-wave to the peak of the positive-going b-wave. Measurements in dark-adapted (scotopic) conditions involved flashes of increasing intensity: 51 dB, −45 dB, −39 dB, −33 dB, −27 dB, −21 dB, −15 dB, −9 dB, −3 dB, and +5 dB. Ten flashes were presented at each intensity, separated by 10 s for steps 1–9 and 20 s

between flashes at the highest intensity. In early experiments, we waited only 10 s between each sweep at the highest intensity but found incomplete recovery from light adaptation between flashes. In later experiments, we therefore lengthened the interval between flashes at the highest intensity to 20 s. Light-adapted (photopic) protocols were performed after background adaptation for 10 min with green light (40 cd/m^2) and conducted with the same background. We tested 6 intensities (−6, −3, 0, 4, 7, and 13 dB) with 25 flashes at each intensity separated by 3 s. Oscillatory potentials were extracted from flash ERGs by bandpass filtering to remove frequency components below 70 Hz and above 280 Hz using an 8-pole Bessel filter in Clampfit (Axon Instruments, Molecular Devices).

2.3. Whole cell recordings

Whole cell recordings from rods were performed using a flatmount preparation of isolated retina. An eye was enucleated immediately after euthanizing the mouse and placed in Ames' medium (US Biological; RRID:SCR_013653) bubbled with 95% O_2/5% CO_2. The cornea was punctured with a scalpel and the anterior segment removed. The retina was isolated by cutting optic nerve attachments. After making four fine cuts at opposite poles, the retina was flattened onto a glass slide in the perfusion chamber with photoreceptors facing up. The retina was anchored in place with a brain slice harp (Warner Instruments, cat. no. 64-0250). The perfusion chamber was placed on an upright fixed-stage microscope (Nikon E600FN) with a 60× water-immersion, long-working distance objective (1.0 NA). Flatmount preparations were superfused with room temperature Ames solution bubbled with 95%/5%CO2 at ~1 mL/min. Outer segments were removed by gentle suction using a patch pipette to expose inner segments for recording.

Patch recording electrodes were pulled on a Narishige (Amityville, NY) PP-830 vertical puller using borosilicate glass pipettes (1.2-mm outer diameter, 0.9-inner diameter with internal filament; World Precision Instruments, Sarasota, FL). Pipettes had tip diameters of 1–2 μm and resistances of 10–15 MΩ. Rod inner segments and cell bodies were identified in flatmount retina and targeted with positive pressure using recording electrodes mounted on Huxley-Wall or motorized micromanipulators (Sutter Instruments). Cones can be distinguished from rods by their larger membrane capacitance and much larger Ca^{2+} currents.

We used two techniques as a presynaptic assay for glutamate release from rods. In the first, we measured glutamate transporter anion currents ($I_{A(Glu)}$) in rods and in the second, we measured exocytotic changes in membrane capacitance.

Rod ribbons are surrounded by the glutamate transporters EAAT2 and EAAT5 (Arriza et al., 1997; Eliasof et al., 1998; Hasegawa et al., 2006) and glutamate reuptake into rods by these transporters activates a large, anion conductance (Arriza et al., 1997; Grant and Werblin, 1996; Rabl et al., 2005; Schneider et al., 2014). $I_{A(glu)}$ is activated during glutamate re-uptake but is thermodynamically uncoupled from the transport process (Machtens et al., 2015). To enhance $I_{A(Glu)}$, Cl^- in the patch pipette was replaced with a more permeable anion, thiocyanate (Eliasof and Jahr, 1996). The intracellular pipette solution for these experiments contained (in mM): 120 KSCN, 10 TEA-Cl, 10 HEPES, 1 CaCl2, 1 MgCl2, 0.5 Na-GTP, 5 Mg-ATP, 5 EGTA, 5 phospho-creatine, pH 7.3. In Ca^{2+} buffering experiments,

we varied the Ca^{2+} chelator concentration: EGTA (0.1 mM, 5 mM) or BAPTA (1 mM, 10 mM). Bath application of the glutamate transport inhibitor DL-*threo*-β-benzyloxyaspartic acid (TBOA; 0.3 mM) blocked depolarization-evoked currents in rods as expected for glutamate transporter anion currents.

Rod $I_{A(glu)}$ recordings were performed in whole-cell voltage clamp using an Axopatch 200B amplifier (Molecular Devices) and signals were digitized with a DigiData 1550 interface (Molecular Devices). Data acquisition and analysis were performed using pClamp 10 software (Molecular Devices). Currents were acquired at 10 kHz and filtered at 2 kHz. Passive membrane resistance was subtracted from $I_{A(Glu)}$ using P/8 subtraction. Membrane capacitance, membrane resistance, and access resistance values for rods using the KSCN solution averaged 3.6 pF ± 0.2, 1.9 ± 0.2 GΩ, and 56 ± 7.9 MΩ (n = 12), respectively.

Capacitance measurements were made with a HEKA EPC-10 amplifier and Patchmaster software (Lambrecht, Pfalz, Germany) using the 'sine + dc' lock-in mode to monitor changes in membrane capacitance, membrane conductance, and series resistance. Lock-in outputs were sampled at 20 kHz and filtered at 2.9 kHz. For these measurements, the pipette solution contained (in mM): 120 CsGluconate, 10 TEA-Cl, 10 HEPES, 2 EGTA, 1 CaCl2, 1 MgCl2, 0.5 Na-GTP, 5 Mg-ATP, 5 phosphocreatine (pH 7.3). Pipettes were coated with dental wax to reduce stray capacitance. We held rods at −70 mV and applied a 2 kHz sine wave (50 mV peak to peak). Baseline levels were measured over a 50–100 ms period prior to the test step. We blanked acquisition during the test step and for 30 ms afterwards to avoid gating and conductance changes. Evoked capacitance changes were then measured from the average capacitance level attained during the subsequent 50–100 ms. With 500 ms test steps that evoked large conductance changes, capacitance changes were sometimes icorrelated with conductance changes. When this occurred, we waited until the conductance change had subsided before measuring the capacitance change.

Voltages were not corrected for liquid junction potentials (KSCN pipette solution: 3.9 mV, CsGluconate pipette solution: 12.3 mV). Chemical reagents were obtained from Sigma-Aldrich unless otherwise indicated.

2.4. Immunohistochemistry

For immunohistochemical experiments, eyes were enucleated after euthanizing the mouse and then placed in oxygenated Ames' medium. After removing the cornea and lens, the posterior eyecup was fixed in 4% paraformaldehyde for 45 min. The eyecup was then washed in PBS 3 times for 10 min each, and cryoprotected in 30% sucrose overnight at 4 °C. Eyecups were embedded in OCT compound (Sakura Finetek USA, Torrance, CA) and stored at −80 °C until sectioning at 25 μm with a cryostat (Leica CM 1800; Chicago, IL). Retinal sections were treated with a blocking solution of 1% Triton X-100 and 6% donkey or goat serum (Jackson Immunoresearch, West Grove, PA and Life Technologies, Carlsbad, CA, respectively) for 3 h before applying the primary antibody. The blocking serum was chosen to match the species in which the secondary antibody was raised. Primary and secondary antibodies (Table 1) were diluted to working concentrations in blocking solution. Sections were incubated in primary antibody at 4 °C overnight and in secondary antibody at

room temperature for 2–3 h. Retinal sections were mounted with Vectashield (Vector Labs, Burlingame CA, RRID: AB_2336787) before imaging.

Confocal imaging was performed using NIS Elements software (Nikon, RRID:SCR_014329) and a spinning disk confocal microscope that consisted of a laser confocal scanhead (PerkinElmer Ultraview LCI, Waltham, MA) equipped with a cooled CCD camera (Hamamatsu Orca ER; Hamamatsu City, Shizuoka, RRID:SCR_017105) mounted on a Nikon E600FN microscope. Fluorescent excitation was delivered from an argon/krypton laser at 488, 568 or 648 nm and emission was collected at 525, 607 and 700 nm, respectively. Filters were controlled using a Sutter Lambda 10–2 filter wheel and controller. The objective (water immersion, 60×, 1.2 NA) was controlled with an E662 z-axis controller (Physik Instrumente; Karlruhe, Germany). Image brightness and contrast were adjusted using Nikon Elements, Fiji, and/or Adobe Photoshop software.

2.5. Western blot analysis

Mouse brain tissue was isolated and homogenized in 1X PBS using a Dounce homogenizer. Tissue was placed in the homogenizer with 1 mL of 1X PBS and homogenized with 10 strokes of the homogenizer. SDS/DTT was added to the brain homogenate (1:1). The homogenate was then transferred to a Falcon tube for storage. Another mL of 1X PBS was added to the empty homogenizer to wash, followed by an additional 10 strokes, which was then added to the previously homogenized tissue. The homogenate was centrifuged at 10,000 RPM × 10 min and supernatant collected. Protein quantification was performed using a Pierce 660 nm Protein Assay with BSA standards. For each sample, 10 μg of protein was separated by SDS-PAGE on NuPAGE 4%–12% Bis-Tris gels (Thermo Fisher Scientific). After electrophoresis, proteins were transferred to a nitrocellulose membrane using an iBlot2 instrument (Invitrogen, Waltham, MA, United States). Membranes were blocked with Tris-buffered saline with 0.1% Tween-20 (TBST)/SuperBlock (Thermo Fisher Scientific, Waltham, MA, United States) for 30 min at RT, and then incubated overnight with Syt7 antibodies (Synaptic Systems, 105–173, 1:500) in TBST/SuperBlock at 4 °C. Blots were washed 3 × 10 min with TBST and then incubated with appropriate secondary antibodies (Licor) for 1 h at RT. Membranes were washed again 3 × 10 min with TBST and imaged on an Odyssey imager (Licor).

2.6. Experimental design and statistical analysis

Statistical analysis and data visualization were done using ClampFit 10 and GraphPad Prism 9 software. Roughly equal numbers of male and female mice were used for these experiments. For ERG measurements and capacitance recordings, we analyzed the sample for each condition using Dunnett's multiple comparisons test with one-way ANOVA. When comparing different test step durations, different genotypes, and different buffers with $I_{A(glu)}$ measurements, we used multiple t-tests with Holm-Sidak correction or 2-way ANOVA with Tukey's test for multiple comparisons. The criterion for statistical significance was set at $\alpha = 0.05$. Data values in the text are reported as mean ± SD. Error bars in Figs. 4, 5 and 6 show 95% confidence intervals.

3. Results

3.1. Syt7 conditional knockout mice

The high affinity Ca^{2+} sensor, Syt7, serves as a sensor for slow, asynchronous release at bipolar cell ribbon synapses as well as several conventional synapses (Bacaj et al., 2013; Luo et al., 2015; MacDougall et al., 2018; Turecek and Regehr, 2018). We tested for Syt7 at photoreceptor synapses using a knockout-verified polyclonal antibody to Syt7 (Synaptic Systems, anti-synaptotagmin 7, 105–173). This antibody labeled both inner and outer plexiform layers of the retina where synaptic terminals of bipolar cells and photoreceptor cells reside, respectively (Fig. 1A). Fig. 1A and B shows sections stained with antibodies to Syt7 and CtBP2. Labeling with the Syt7 antibody was abolished by pre-incubation with the fusion peptide used for immunization to generate the antibody (Synaptic Systems, Syt7 105-71P; Fig. 1C). Antibodies to CtBP2 label the Ribeye protein that forms synaptic ribbons as well as a shorter, non-ribbon form of CtBP2 found in cell bodies (Schmitz et al., 2000). A row of small ribbons in Fig. 1B belonging to a cone pedicle (arrow) are interspersed among numerous ribbons belonging to rod spherules. This cone pedicle was labeled by Syt7 antibodies (arrow, merge image). The section in Fig. 1D was stained with antibodies to Syt7 (red) and FITC-conjugated peanut agglutinin (PNA; green). PNA stains the cone pedicle base and so this image provides further evidence that Syt7 antibodies (Fig. 1 D, merge, arrows) labeled cone pedicles. Punctate rod terminals that show weaker PNA staining were also labeled by Syt7 antibodies. Fig. 1E shows the OPL co-stained with antibodies to Syt7 and vesicle protein SV2. Overlap of these antibodies in the merged image provides further evidence that Syt7 is present in photoreceptor terminals. As we consider in the Discussion, this overlap also raises the possibility that Syt7 may be present on vesicle membranes.

To test a role for Syt7 in release from rods, we generated mice to allow conditional knockouts of Syt7. Fig. 2A illustrates the wild-type locus and floxing design for targeting exon 5 of Syt7 (variant 201). The floxed allele was generated with the *Easi*-CRISPR method (Quadros et al., 2017; Miura et al., 2018) that uses long single-stranded DNA as the repair donor template. *LoxP* sites flanked exon 5 and included part of the first calcium-binding C2A domain. Protocols for mouse zygote injections used for generating founder mice are described elsewhere (Harms et al., 2014; Miura et al., 2018). Genotyping of the F0 offspring using PCR for each of the two *LoxP* sites is shown in Fig. 2B. PCR-RFLP (Restriction Fragment Length Polymorphism) with EcoRI digestion was used to further confirm correctly targeted mice (Fig. 2C). Sequences of the Syt7 repair template, guide RNA, and genotyping primers are provided in Supplementary Data (Appendix A).

The two genotyping assays (B and C) showed that animals #5 and #11 contain correctly targeted floxed alleles. Animal #6 contained only the 5' *LoxP* site and animals #8 and 9 showed deletion of the targeted region. Founders 5 and 11 were bred to establish the floxed mice colonies. Founder 9 was bred to establish Syt7 knockout mouse colonies by crossing with C57/BL6J mice. We used these whole animal Syt7 knockout mice for ERG experiments. However, like an earlier Syt7 knockout mouse line (Chakrabarti et al., 2003), these mice did not breed well and we lost the line soon thereafter. For later experiments, we created another whole animal knockout by crossing $Syt7^{fl/fl}$ mice with mice expressing cre-

recombinase ubiquitously using the CMV promoter (CMV-Cre, B6.C-Tg(CMV-cre)1Cgn/J). Also like the earlier Syt7 knockout mouse line (Chakrabarti et al., 2003), $Syt7^{fl/fl/CMVcre}$ mice did not differ significantly in weight from age-matched, littermate heterozygotes (df = 25; t = 0.21, p = 0.84, 9 $Syt7^{fl/fl/CMVcre}$ vs. 18 heterozygous controls, nested *t*-test). Western blot of whole brain protein showed an absence of protein at the expected molecular weight of ~45 kD in homozygous $Syt7^{fl/fl/CMVcre}$ mice with no changes evident in heterozygous or Cre-negative $Syt7^{fl/fl}$ mice compared to a C57Bl6 control mouse (Fig. 2D).

We examined sensitivity of Syt7 labeling in the retina to selective elimination of Syt7 using immunohistochemistry. Like the Synaptic Systems antibody in Fig. 1, a Neuromab antibody to Syt7 labeled both the IPL and OPL in control mice (Fig. 3A). To generate mice lacking Syt7 from both rod and cone terminals, we crossed $Syt7^{fl/fl}$ mice with HRGP-Cre and Rho-iCre mice. In these mice, Syt7 labeling was largely eliminated from the OPL while labeling remained in the IPL (Fig. 3B). These sections were co-stained with FITC-conjugated PNA to label cone terminals. Labeling of the OPL can be seen more clearly in the magnified images in Fig. 3C and D. In a global Syt7 knockout created by crossing $Syt7^{fl/fl}$ mice with CMV-cre mice, Syt7 labeling was eliminated from both the OPL and IPL (Fig. 3F). Labeling with the Synaptic Systems Syt7 antibody was also abolished in the OPL and IPL in these same $Syt7^{KO}$ mice (Fig. 3H). These data further confirm cre-dependent excision of Syt7 in $Syt7^{fl/fl}$ mice.

3.2. Release from individual rods

We used whole cell patch clamp recording techniques to test the role of Syt7 in release from rods. We took advantage of the fact that glutamate release from rods can be measured presynaptically by recording anion currents generated during glutamate re-uptake ($I_{A(Glu)}$) via EAAT transporters (Hasegawa et al., 2006; Szmadja and Devries 2011). $I_{A(glu)}$ is linearly related to glutamate levels in the cleft making it a useful presynaptic assay for release (Otis and Jahr, 1998). Fig. 4A–C shows examples of $I_{A(glu)}$ evoked by depolarizing test steps of various durations applied to rods in a retinal flatmount preparation. We measured the amplitude of $I_{A(glu)}$ ~2 ms after termination of the test step to allow time for Ca^{2+} currents to de-activate (Grabner and Moser, 2021) and avoid any residual capacitative currents that might remain after P/6 subtraction of passive properties. We waited 45 s between trials and varied the sequence of test step durations among experiments. Rundown of release capability was rapid and we typically obtained only a few measurements from each rod.

We analyzed sites of glutamate release involved in different components of release by recording from rods using different intracellular Ca^{2+} buffers introduced through the patch recording pipette. Fig. 4A, B and C show example recordings from control mice under four different buffering conditions (0.1 mM EGTA, 5 mM EGTA, 1 mM BAPTA, and 10 mM BAPTA) with depolarizing steps of 5, 25, and 500 ms, respectively. We chose these step durations to distinguish fast and slow components of release. Fig. 4D plots $I_{A(glu)}$ amplitude as a function of step duration with these different buffers. BAPTA and EGTA bind Ca^{2+} with similar affinities, but BAPTA binds it much more rapidly, thus constraining Ca^{2+} increases to locations very close to the site of entry (Adler et al., 1991). Our standard pipette solution used 5 mM EGTA as the Ca^{2+} buffer (filled black circles). Using 1 mM BAPTA as the

exogenous Ca^{2+} buffer in the pipette solution restricts the spread of Ca^{2+} to nanodomains within ~100 nm of Ca^{2+} channels. With this buffer, currents evoked by 5 and 25 ms (red open triangles, Fig. 4D) were similar to those seen with 5 mM EGTA (black filled circles), but 1 mM BAPTA prevented further increases in $I_{A(glu)}$ with 500 ms steps (red open triangles). Buffering Ca^{2+} more strongly with 10 mM BAPTA eliminated $I_{A(Glu)}$ at all step durations by immediately buffering Ca^{2+} that entered through voltage-gated Ca^{2+} channels before it could reach any release sites (blue filled triangles). When using 0.1 mM EGTA to provide only weak Ca^{2+} buffering, responses evoked by 5 ms steps were unchanged, but responses to longer steps were enhanced (gray open circles). Lengthy tail currents were often evoked by 500 ms steps when using 0.1 mM EGTA. While tail currents were almost fully blocked by the glutamate transport inhibitor, TBOA (0.3 mM) (Grassmeyer et al., 2019, Fig. 5), it is nevertheless likely some Ca^{2+}-activated Cl^- channels were also activated with weak buffering and sustained Ca^{2+} influx.

These data suggest that fast synchronous release evoked by short 5 ms test steps involves vesicles located within Ca^{2+} nanodomains very close to Ca^{2+} channels, whereas release evoked by maintained Ca^{2+} entry accompanying longer steps recruited additional release from more distant sites. Ca^{2+} channels cluster beneath synaptic ribbons in rods and cones (Lv et al., 2012; Morgans et al., 2005; Morgans, 2001; Nachman-Clewner et al., 1999; tom Dieck et al., 2005) suggesting that the fast, synchronous release of synaptic vesicles evoked by brief depolarizing stimuli occurs predominantly at ribbons, whereas release evoked by longer depolarizing steps engages release sites further from ribbon-associated Ca^{2+} channels (Mercer et al., 2011).

3.3. Release from individual rods: roles of Syt1 and Syt7

Using the mouse lines described above, we examined the roles of Syt1 and Syt7 in fast and slow components of release from rods. Fig. 5A, B, and C show example recordings of responses to 5, 25, and 500 ms from rods in which Syt1 and/or Syt7 have been eliminated. Fig. 5D, E, and F plot $I_{A(glu)}$ amplitude as a function of duration. Inward currents evoked at the end of 25 and 500 ms test steps were blocked by the glutamate transport inhibitor, TBOA (0.3 mM), confirming that these currents arise from glutamate transporters (filled triangles, Fig. 5D).

As illustrated in Fig. 5, eliminating Syt1 from rods (red traces) reduced the amplitude of $I_{A(Glu)}$ evoked by 5 and 25 ms steps relative to $I_{A(Glu)}$ measured in control mouse rods ($p = 0.0013$, Tukey's multiple comparisons test; Fig. 5D). Eliminating Syt1 did not reduce the amplitude of currents measured after termination of 500 ms steps (Fig. 5).

We then recorded from rods in which Syt7 had been selectively eliminated using $Rod^{Syt7CKO}$ mice. Eliminating Syt7 from rods had a complementary effect to elimination of Syt1: no effect on $I_{A(Glu)}$ evoked by 5 and 25 ms steps but a reduction in the amplitude of currents evoked by 500 ms steps (gray traces, Fig. 5A–C; gray diamonds, Fig. 5D).

We also recorded from rods in mice where we eliminated both Syt1 and Syt7 ($Rod^{Syt1/Syt7CKO}$). In the absence of both sensors, $I_{A(Glu)}$ amplitude was significantly reduced at all step durations (blue traces, Fig. 5A–C; blue open squares, Fig. 5D; p

= 0.0273). Residual currents that remained after eliminating both sensors did not differ significantly in amplitude from currents that remained in control mice after blocking glutamate transporters with TBOA (0.3 mM; black triangles, Fig. 5D).

Ca^{2+} buffering experiments indicated that fast release occurs at ribbon-associated release sites whereas slow release involves sites further away from ribbon-associated Ca^{2+} channels suggesting that Syt1 is used primarily at ribbon release sites and Syt7 at non-ribbon sites. To test this idea further, we varied Ca^{2+} buffering in $Rod^{Syt1CKO}$ and $Rod^{Syt7CKO}$ mice. Fig. 5E shows effects of 1 mM and 10 mM BAPTA in $Rod^{Syt1CKO}$ mice, along with responses of $Rod^{Syt1CKO}$ rods recorded with 5 mM EGTA (filled red squares) for comparison. Restricting the spread of intracellular Ca^{2+} by using 1 mM BAPTA (open red squares, Fig. 5E) significantly reduced amplitude of currents evoked by 500 ms steps in rods of $Rod^{Syt1CKO}$ mice, providing evidence that the presence of Syt7 alone is sufficient to support release from non-ribbon sites. As with control rods, elevating BAPTA further to 10 mM (asterisks, Fig. 5E) abolished IA(glu) in $Rod^{Syt1CKO}$ mice.

We next tested effects of lowering Ca^{2+} buffering to 0.1 mM EGTA in $Syt7^{KO}$ mice (CMV^{Syt7KO}). In rods from $Syt7^{KO}$ mice (open gray triangles), the increase in $I_{A(glu)}$ amplitude seen in control rods (open black circles, Fig. 5F) with 25 and 500 ms steps when using 0.1 mM EGTA was abolished (Fig. 5F). In addition to providing further evidence that Syt7 mediates release from non-ribbon sites, the finding that $I_{A(glu)}$ no longer increased with longer steps in the absence of Syt7 suggests that additional Syt1-mediated slow release from more distant sites is not engaged even when Ca^{2+} buffering is reduced.

Rates of spontaneous vesicle release in rods held at −70 mV were unchanged by eliminating Syt7 (0.43 ± 0.47 vesicles/s; n = 14) when compared to control (0.40 ± 0.30 vesicles/s, SD; n = 50; p = 0.78, unpaired *t*-test). Consistent with earlier results, spontaneous release rates were elevated in rods lacking Syt1 (Grassmeyer et al., 2019; Hays et al., 2020). However, simultaneous elimination of both Syt1 and Syt7 from rods did not alter release rates compared to elimination of Syt1 alone ($Rod^{Syt1CKO}$, 4.2 ± 2.3 quanta/s, n = 9; $Rod^{Syt1/Syt7CKO}$, 3.57 ± 2.26 quanta/s; p = 0.73, unpaired *t*-test; $Rod^{Syt1CKO}$ data from Hays et al., 2020, Fig. 8). Profuse spontaneous release persisted in rods from $Rod^{Syt1CKO}$ mice even when using 10 mM BAPTA as the intracellular Ca^{2+} buffer (2.5 ± 1.82 quanta/s, p = 0.176, unpaired *t*-test) and did not differ significantly from rod recordings obtained with 5 mM EGTA from $Rod^{Syt1CKO}$ mice. This suggests that much of the spontaneous release that occurs in the absence of Syt1 involves Ca^{2+}-independent mechanisms.

3.4. Capacitance recordings from rods

As a second means of testing the roles of Syt1 and Syt7 in release from rods, we used membrane capacitance recordings. Synaptic vesicle release increases membrane surface area and thereby increases total membrane capacitance. Because they possess only a single ribbon, rods release only a small number of vesicles upon stimulation and thus generate only small capacitance increases. Fig. 6A shows example recordings of changes in membrane capacitance (C_m), membrane conductance (G_m) and access conductance (G_s) following depolarizing steps (−70 to −10 mV) of 10 and 100 ms applied to rods from control, $Rod^{Syt1CKO}$, and $Syt7^{KO}$ mice. Assuming a single vesicle capacitance of 38 aF (Grabner and

Moser, 2021), the average capacitance jump in control rods of 3.86 ± 2.67 fF (n = 24 rods) evoked by 10 ms steps to −10 mV equates to release of ~100 vesicles, consistent with a previous report (Grabner and Moser, 2021).

Consistent with $I_{A(glu)}$ measurements, eliminating Syt1 from rods in $Rod^{Syt1CKO}$ mice abolished release evoked by 5 ms steps (**, p = 0.004, *t*-test corrected for multiple comparisons, false discovery rate approach; Fig. 6). Release evoked by longer steps was reduced by half. Consistent with a role in a slower component of release, eliminating Syt7 from rods in Syt7KO mice had only a small effect at 5 and 10 ms but halved release with longer steps (Fig. 6). Capacitance jumps in both mouse strains differed significantly from control mouse rods (Control vs. $Rod^{Syt1CKO}$ mice: $p < 0.0001$. Control vs. Syt7KO: p = 0.0043; Dunnett's multiple comparisons test).

We saw no evidence for significant endocytic retrieval during the first 200 ms and so exocytotic increases in membrane capacitance over that period provide a measure of cumulative release. By contrast, $I_{A(glu)}$ is only active for as long as glutamate remains bound to the transporter. As a consequence, single vesicle $I_{A(glu)}$ events decline a time constant of ~50 ms (Hays et al., 2020) and so $I_{A(glu)}$ measurements provide a snapshot of release occurring over the previous ~50 ms. Unlike $I_{A(glu)}$ measurements that decline more quickly, Syt1-mediated release that occurred at the beginning of a long step generate capacitance increases that are largely maintained throughout the step, even in the absence of Syt7 (Fig. 6). Summing the capacitance changes seen in the two genetically modified mouse lines restored the amplitude/duration relationship to control values (open gray squares, Fig. 6).

3.5. ERG recordings

To study the roles of Syt1 and Syt7 in synaptic transmission and shaping bipolar cell light responses, we measured ERGs in vivo from anesthetized mice. Fig. 7A shows representative ERG responses evoked by a high intensity 20 ms flash applied to dark-adapted mice under scotopic conditions. B-waves reflect the responses of second-order ON-type bipolar cells and a-waves provide a measure of photoreceptor responses. Fig. 7B and C plot the amplitude of scotopic a- and b-waves, respectively, as a function of flash intensity for several mouse lines. Fig. 7D shows examples of photopic b-waves and Fig. 7E plots the amplitude of photopic b-waves. While the scotopic ERG arises from a combination of rod and cone inputs, the photopic ERG obtained under light-adapted conditions arises purely from cones.

We used the ERG to test the role of Syt7 in shaping light-evoked responses of rod bipolar cells. In global Syt7 knockout mice, we saw a small reduction in b-waves, with larger decreases at higher intensities (Fig. 7C). To determine whether these changes arose from rods, we tested mice in which Syt7 was selectively eliminated from rods ($Rod^{Syt7CKO}$). Unlike the global Syt7 knockout, mice lacking Syt7 only in rods did not show diminished b-waves compared to controls (Fig. 7C). There was also no significant reduction in scotopic a-waves (Fig. 7B) or photopic b-waves (Fig. 7E).

Consistent with ERG recordings performed using isolated retinas (Grassmeyer et al., 2019), these whole animal recordings showed that eliminating Syt1 from rods using $Rod^{Syt1CKO}$ mice diminished scotopic b-wave amplitude across the entire intensity range compared to

controls (Fig. 7C). Surprisingly, in mice lacking Syt1 in rods, there was no further reduction in ERG b-waves caused by the added elimination of Syt7 from rods ($Rod^{Syt1Syt7CKO}$) (Fig. 7C).

Eliminating Syt1 from cones in $Cone^{Syt1CKO}$ mice also reduces scotopic ERG b-waves (Grassmeyer et al., 2019). We generated mice in which Syt1 was removed from both rods and cones by crossing $Rod^{Syt1CKO}$ mice with $Cone^{Syt1CKO}$ mice to create Rod/$Cone^{Syt1CKO}$ mice. As illustrated by the example in Fig. 7A, scotopic B-waves were almost completely abolished in these mice. Summary measurements of b-wave amplitude are plotted in Fig. 7C. Scotopic a-waves were comparable, indicating that the reduced b-waves were not due to diminished photoreceptor light responses (Fig. 7B). As expected from earlier experiments in isolated retina suggesting that Syt1 is the principal Ca^{2+} sensor used by cones (Grassmeyer et al., 2019), photopic ERG b-waves were eliminated in mice lacking Syt1 in both rods and cones (Rod/$Cone^{Syt1CKO}$, Fig. 7E).

Finally, we tested mice lacking Syt1 and Syt7 in both rods and cones (Rod/$Cone^{Syt1Syt7CKO}$). Representative scotopic and photopic ERGs are shown in Fig. 7A and D. There was no further decrease in scotopic b-waves in these mice compared to Rod/$Cone^{Syt1CKO}$ mice that lacked Syt1 but retained Syt7 in rods and cones (Fig. 7C). Like Rod/$Cone^{Syt1CKO}$, the photopic b-wave was also eliminated in these mice (Fig. 7E). Together, these data show that eliminating Syt7 from rods has little or no effect on the ERG b-wave.

3.6. Syt7 and oscillatory potentials

Given robust labeling of the IPL by antibodies to Syt7 (Fig. 1), we looked at effects in Syt7KO mice on ERG oscillatory potentials that arise from interactions with amacrine cells (Wachtmeister, 1998). Along with the small reduction in b-waves shown in Fig. 7C, oscillatory potentials were also reduced in Syt7 KO mice (Fig. 8). Fig. 8A overlays scotopic ERG responses to a bright flash in control C57Bl6 and Syt7 KO mice. As illustrated in Fig. 8B, oscillatory potentials were isolated from a- and b-waves by bandpass filtering to remove frequencies below 70 Hz and above 280 Hz. Oscillatory potentials evoked by flashes applied in scotopic conditions were diminished by eliminating Syt7 (samples compared by mixed effects analysis: $P < 0.0001$; individual comparisons significant at −9 dB, $P = 0.00059$ and −3 dB, $P = 0.00325$; unpaired *t*-test corrected for multiple comparisons, Holm-Sidak method; Fig. 8C, circles). Interestingly, oscillatory potentials evoked in photopic conditions were unchanged (Fig. 8C, triangles), suggesting that effects of Syt7 are largely restricted to neurons in the rod pathway, although oscillatory potentials were not reduced in $Rod^{Syt7CKO}$ mice (not shown). The latency to the largest positive peak in the oscillatory potentials (arrow in panel B) was unchanged in scotopic (Fig. 8D) and photopic conditions (data not shown) by elimination of Syt7.

4. Discussion

Earlier studies in salamander and mouse retina showed that inhibiting CICR to reduce non-ribbon release from rods led to a substantial reduction in bipolar and horizontal cell light responses (Babai et al., 2010; Cadetti et al., 2006; Suryanaryanan and Slaughter, 2006; Grabner and Moser, 2021). This suggested that non-ribbon release from rods might play

an important role in encoding light responses at the synapse. In the present study, single rod recordings of $I_{A(glu)}$ and membrane capacitance changes both support the conclusion that Syt1 drives fast release at ribbon-associated sites in rods whereas Syt7 primarily drives release at more distant non-ribbon sites that can be evoked by lengthy depolarizing steps. Surprisingly, eliminating Syt7 from rods had little or no effect on the ERG b-wave. Moreover, in the absence of Syt1 in both rods and cones, Syt7 was unable to support a significant b-wave.

Glutamate release and exocytotic membrane capacitance jumps evoked in rods by brief steps were both largely abolished by eliminating Syt1 whereas eliminating Syt7 preferentially reduced release evoked by longer steps. When Syt7 was present in rods, release evoked by longer steps was enhanced by lowering Ca^{2+} buffering to 0.1 mM EGTA and inhibited more strongly by 1 mM BAPTA than by 5 mM EGTA. When Syt7 was eliminated but Syt1 remained in rods, lower Ca^{2+} buffering did not enhance release. Together, these data suggest that brief steps evoke fast, synchronous vesicle release involving ribbon-associated vesicles and the Ca^{2+} sensor Syt1 whereas Syt7 is the main sensor controlling a slower form of release from more distant, non-ribbon sites. Increasing the spread of Ca^{2+} by using longer steps or weaker Ca^{2+} buffering enhances Syt7-mediated release, similar to results from retinal bipolar cells (Luo et al., 2015). One caveat is that most of our control recordings were done with wild-type rather than $Syt7^{fl/fl}$ mice that lacked cre-recombinase.

Syt1 and Syt7 reside at the same synapses in many neurons (MacDougall et al., 2018). It has been proposed that Syt7 on adjacent plasma membranes may lower the energy barrier for fusion to facilitate Syt1-mediated vesicle fusion (Jackman et al., 2016). Syt7 has a higher Ca^{2+} affinity than Syt1 and so this hypothesis assumes that Syt7 is less effective by itself than Syt1 at promoting fusion. A greater propensity for fusion could explain why Syt1 is the principal sensor that drives fusion near ribbon-associated Ca^{2+} channels where Ca^{2+} can reach high levels. Even assuming a lower propensity for fusion, the higher Ca^{2+} sensitivity of Syt7 could support fusion at distant, non-ribbon sites where Ca^{2+} is generally lower. This hypothesis also predicts that elevating Ca^{2+} at sites far from the ribbon should promote Syt1-mediated fusion at these sites. One way to achieve this would be Ca^{2+} release from intracellular stores. We have not yet investigated interactions between these sensors and CICR, but if CICR can drive Syt1-mediated fusion at non-ribbon sites, then this might explain why release from rods is sensitive to inhibition of CICR (Chen et al., 2014; Babai et al., 2010; Cadetti et al., 2006; Chanaday et al., 2021; Suryanaryanan and Slaughter, 2006; Szikra et al., 2008, 2009). This could reconcile these earlier results with the present findings that eliminating Syt1 with or without Syt7 is sufficient to extinguish ERG b-waves.

4.1. Effects on spontaneous release

Like many neurons, eliminating Syt1 elevates the rate of spontaneous vesicle release in rods held at −70 mV (Grassmeyer et al., 2019; Schneggenburger and Rosenmund, 2015). These results support the idea that Syt1 acts as a fusion clamp to limit spontaneous fusion. We found that spontaneous fusion rates remained high even with 10 mM BAPTA in the pipette that blocks evoked release suggesting that spontaneous release in the absence of Syt1 is Ca^{2+}-independent. Syt7 has also been suggested to function as a fusion clamp, although

weaker than Syt1 because of its greater Ca^{2+} sensitivity (MacDougall et al., 2018). However, we did not see any significant change in spontaneous rates following loss of Syt7, consistent with a report on hippocampal neurons (Bourgeois-Jaarsma et al., 2021).

4.2. Possible roles of Syt7

Syt7 is expressed in many neurons as well as many other cell types (MacDougall et al., 2018; Huson and Regehr, 2020). In neurons, Syt7 can promote asynchronous release of synaptic vesicles, vesicle replenishment, and paired pulse facilitation. The slow form of release in our studies evoked by lengthy depolarizing steps is not the same as asynchronous release defined at other synapses, which is characterized by the delayed fusion of vesicles after a single brief stimulus. However, the characteristics of Syt7-mediated release in rods are similar to the slow form of release promoted by Syt7 in rod bipolar cells (Luo et al., 2015).

Syt7 is found on the plasma membrane of many CNS synapses, but also on vesicle membranes in neuroendocrine cells (MacDougall et al., 2018; Vevea et al., 2021). Furthermore, Syt1 and Syt7 segregate to spatially and functionally distinct populations of large dense core granules (Rao et al., 2014, 2017). Overlap between Syt7 labeling and the vesicle marker SV2 in rod terminals raises the possibility that Syt7 may likewise reside on vesicle membranes in rods, even perhaps in vesicles distinct from Syt1. Unfortunately, labeling by Syt7 antibodies was not sufficiently robust for definitive subcellular localization of Syt7 in small rod spherules.

Immunohistochemical experiments showed evidence for Syt7 in both inner and outer plexiform layers of the retina where synaptic terminals of bipolar cells and photoreceptors reside, respectively (Fig. 1). Labeling for Syt7 in the IPL is consistent with physiological evidence for Syt7 in rod ON bipolar cells (Luo et al., 2015). However, labeling in the IPL was not limited to the ON sublamina of the IPL but also present in the distal half where OFF bipolar cells terminate. The finding that ERG oscillatory potentials were reduced after global elimination of Syt7 suggests that amacrine cells may also use Syt7 (Wachtmeister, 1998). Oscillatory potentials were reduced only under scotopic conditions, suggesting Syt7 contributions are largely restricted to rod-driven circuits. In addition to direct effects on rod bipolar cells (Luo et al., 2015), the reduction in scotopic b-waves seen in global Syt7 knockout mice might also involve modulation of rod bipolar cell activity by amacrine cells (Smith et al., 2013).

What is the role of non-ribbon release in rods? One possibility is that release at non-ribbon sites may act preferentially on horizontal cell dendrites that flank bipolar cell dendrites in the invaginating rod synapse. Another possibility is that non-ribbon release may modulate basal levels of glutamate in the cleft and thereby regulate the activity of glutamate transporters and/or pre- and post-synaptic glutamate receptors (Veruki et al., 2006; Hellmer et al., 2018; Koulen and Brandstatter, 2002; Nakajima et al., 1993). High cleft glutamate levels are needed to maintain mGluR6 receptors near saturation for the non-linear thresholding mechanism employed by rod bipolar cells in discriminating single photon voltage responses from noise (Field and Rieke, 2002; Hays et al., 2021; Sampath and Rieke, 2004). Light-dependent changes in sustained release could offer a mechanism for

altering this threshold with changing light levels. Changes in cleft glutamate levels might also regulate release by acting on presynaptic metabotropic glutamate receptors to alter intracellular signaling or acting on $I_{A(glu)}$ to alter membrane potential (Hellmer et al., 2018; Koulen and Brandstatter, 2002).

5. Conclusions

Our results show that the sustained release of vesicles from rods and cones in darkness is regulated by the exocytotic Ca^{2+} sensor, Syt1, on vesicles located within 100 nm of ribbon-associated Ca^{2+} channels. Ongoing release from photoreceptors in darkness is thus tightly synchronized with Ca^{2+} channel activity and should not be viewed as a form of asynchronous release as defined at other CNS synapses (Huson and Regehr, 2020). However, like a number of other CNS synapses, including rod bipolar cells (Luo et al., 2015), we found evidence for a form of slow release from rods mediated by Syt7 that involves non-ribbon sites further away from Ca^{2+} channels. Despite prior evidence suggesting non-ribbon release may have a more significant role (Babai et al., 2010; Cadetti et al., 2006; Suryanarayanan and Slaughter, 2006), our studies indicates that Syt7-mediated slow release does not play a significant role in mediating light responses but may instead play a modulatory role. Syt1-mediated fast release allows rod and cone synapses to track changes in light intensity rapidly and accurately. Cones show rapid release kinetics matched to their light response kinetics (Schnapf and Copenhagen, 1982), but the ability for rapid release is also important for rods, especially under mesopic conditions when rod responses can be faster than cones (Pasquale et al., 2020). Reliance on fast release mediated by Syt1 can improve the match between release and light response kinetics, enhancing the ability of the synapse to track rapid, light-dependent changes in membrane potential.

Supplementary Material

Refer to Web version on PubMed Central for supplementary material.

Acknowledgments

The authors thank the UNMC Mouse Genome Engineering core facility for generating transgenic mouse models and Dr. Yun Le (Univ. of Oklahoma Health Sciences Center) for HRGP-Cre mice.

Funding

Funding provided by NIH grants EY10542 and EY32396 to WT, R35HG010719 and R21GM129559 to CBG, EY28848 to JG, and UNMC Graduate Fellowship to CH. The authors declare no competing financial interests.

Data availability

Data will be made available on request.

Abbreviations:

G_s	Access conductance
CICR	Ca^{2+}-induced Ca^{2+} release

TBOA	DL-threo-β-benzyloxyaspartic acid
ERG	Electroretinogram
$I_{A(Glu)}$	Glutamate transporter anion current
C_m	Membrane capacitance
G_m	Membrane conductance
PNA	Peanut agglutinin
Syt1	Synaptotagmin-1
Syt7	Syntaptotagmin-7

References

Adler EM, Augustine GJ, Duffy SN, Charlton MP, 1991. Alien intracellular calcium chelators attenuate neurotransmitter release at the squid giant synapse. J. Neurosci. 11, 1496–1507. [PubMed: 1675264]

Arriza JL, Eliasof S, Kavanaugh MP, Amara SG, 1997. Excitatory amino acid transporter 5, a retinal glutamate transporter coupled to a chloride conductance. Proc. Natl. Acad. Sci. U. S. A. 94, 4155–4160. [PubMed: 9108121]

Babai N, Morgans CW, Thoreson WB, 2010. Calcium-induced calcium release contributes to synaptic release from mouse rod photoreceptors. Neuroscience 165, 1447–1456. [PubMed: 19932743]

Bacaj T, Wu D, Yang X, Morishita W, Zhou P, Xu W, Malenka RC, Sudhof TC, 2013. Synaptotagmin-1 and synaptotagmin-7 trigger synchronous and asynchronous phases of neurotransmitter release. Neuron 80, 947–959. [PubMed: 24267651]

Bourgeois-Jaarsma Q, Miaja Hernandez P, Groffen AJ, 2021. Ca(2+) sensor proteins in spontaneous release and synaptic plasticity: limited contribution of Doc2c, rabphilin-3a and synaptotagmin 7 in hippocampal glutamatergic neurons. Mol. Cell. Neurosci. 112, 103613. [PubMed: 33753311]

Cadetti L, Bryson EJ, Ciccone CA, Rabl K, Thoreson WB, 2006. Calcium-induced calcium release in rod photoreceptor terminals boosts synaptic transmission during maintained depolarization. Eur. J. Neurosci. 23, 2983–2990. [PubMed: 16819987]

Chakrabarti S, Kobayashi KS, Flavell RA, Marks CB, Miyake K, Liston DR, Fowler KT, Gorelick FS, Andrews NW, 2003. Impaired membrane resealing and autoimmune myositis in synaptotagmin VII-deficient mice. J. Cell Biol. 162, 543–549. [PubMed: 12925704]

Chanaday NL, Nosyreva E, Shin OH, Zhang H, Aklan I, Atasoy D, Bezprozvanny I, Kavalali ET, 2021. Presynaptic store-operated Ca(2+) entry drives excitatory spontaneous neurotransmission and augments endoplasmic reticulum stress. Neuron 109, 1314–1332 e1315. [PubMed: 33711258]

Chen M, Krizaj D, Thoreson WB, 2014. Intracellular calcium stores drive slow non-ribbon vesicle release from rod photoreceptors. Front. Cell. Neurosci. 8, 20. [PubMed: 24550779]

Chen M, Van Hook MJ, Zenisek D, Thoreson WB, 2013. Properties of ribbon and non- ribbon release from rod photoreceptors revealed by visualizing individual synaptic vesicles. J. Neurosci. 33, 2071–2086. [PubMed: 23365244]

Eliasof S, Arriza JL, Leighton BH, Amara SG, Kavanaugh MP, 1998. Localization and function of five glutamate transporters cloned from the salamander retina. Vis. Res. 38, 1443–1454. [PubMed: 9667010]

Eliasof S, Jahr CE, 1996. Retinal glial cell glutamate transporter is coupled to an anionic conductance. Proc. Natl. Acad. Sci. U. S. A. 93, 4153–4158. [PubMed: 8633032]

Field GD, Rieke F, 2002. Nonlinear signal transfer from mouse rods to bipolar cells and implications for visual sensitivity. Neuron 34, 773–785. [PubMed: 12062023]

Grabner CP, Moser T, 2021. The mammalian rod synaptic ribbon is essential for Cav channel facilitation and ultrafast synaptic vesicle fusion. Elife 10, e63844. [PubMed: 34617508]

Grant GB, Werblin FS, 1996. A glutamate-elicited chloride current with transporter-like properties in rod photoreceptors of the tiger salamander. Vis. Neurosci. 13, 135–144. [PubMed: 8730995]

Grassmeyer JJ, Cahill AL, Hays CL, Barta C, Quadros RM, Gurumurthy CB, Thoreson WB, 2019. Ca(2+) sensor synaptotagmin-1 mediates exocytosis in mammalian photoreceptors. Elife 8, e45946. [PubMed: 31172949]

Harms DW, Quadros RM, Seruggia D, Ohtsuka M, Takahashi G, Montoliu L, Gurumurthy CB, 2014. Mouse Genome editing using the CRISPR/cas system. Curr Protoc Hum Genet 83, 15 17 11–27.

Hasegawa J, Obara T, Tanaka K, Tachibana M, 2006. High-density presynaptic transporters are required for glutamate removal from the first visual synapse. Neuron 50, 63–74. [PubMed: 16600856]

Hays CL, Sladek AL, Field GD, Thoreson WB, 2021. Properties of multivesicular release from mouse rod photoreceptors support transmission of single-photon responses. Elife 10, e67446. [PubMed: 33769285]

Hays CL, Sladek AL, Thoreson WB, 2020. Resting and stimulated mouse rod photoreceptors show distinct patterns of vesicle release at ribbon synapses. J. Gen. Physiol. 152, e202012716. [PubMed: 33175961]

Hellmer CB, Clemons MR, Nawy S, Ichinose T, 2018. A group I metabotropic glutamate receptor controls synaptic gain between rods and rod bipolar cells in the mouse retina. Phys. Rep. 6, e13885.

Huson V, Regehr WG, 2020. Diverse roles of Synaptotagmin-7 in regulating vesicle fusion. Curr. Opin. Neurobiol. 63, 42–52. [PubMed: 32278209]

Jackman SL, Turecek J, Belinsky JE, Regehr WG, 2016. The calcium sensor synaptotagmin 7 is required for synaptic facilitation. Nature 529, 88–91. [PubMed: 26738595]

Jin N, Zhang Z, Keung J, Youn SB, Ishibashi M, Tian LM, Marshak DW, Solessio E, Umino Y, Fahrenfort I, Kiyama T, Mao CA, You Y, Wei H, Wu J, Postma F, Paul DL, Massey SC, Ribelayga CP, 2020. Molecular and functional architecture of the mouse photoreceptor network. Sci. Adv. 6, eaba7232. [PubMed: 32832605]

Koulen P, Brandstatter JH, 2002. Pre- and postsynaptic sites of action of mGluR8a in the mammalian retina. Invest. Ophthalmol. Vis. Sci. 43, 1933–1940. [PubMed: 12037002]

Krizaj D, Lai FA, Copenhagen DR, 2003. Ryanodine stores and calcium regulation in the inner segments of salamander rods and cones. J. Physiol. 547, 761–774. [PubMed: 12562925]

Le YZ, Ash JD, Al-Ubaidi MR, Chen Y, Ma JX, Anderson RE, 2004. Targeted expression of Cre recombinase to cone photoreceptors in transgenic mice. Mol. Vis. 10, 1011–1018. [PubMed: 15635292]

Li S, Chen D, Sauve Y, McCandless J, Chen YJ, Chen CK, 2005. Rhodopsin-iCre t ransgenic mouse line for Cre-mediated rod-specific gene targeting. Genesis 41, 73–80. [PubMed: 15682388]

Luo F, Bacaj T, Sudhof TC, 2015. Synaptotagmin-7 is essential for Ca2+-triggered delayed asynchronous release but not for Ca2+-dependent vesicle priming in retinal ribbon synapses. J. Neurosci. 35, 11024–11033. [PubMed: 26245964]

Lv C, Gould TJ, Bewersdorf J, Zenisek D, 2012. High-resolution optical imaging of zebrafish larval ribbon synapse protein RIBEYE, RIM2, and CaV 1.4 by stimulation emission depletion microscopy. Microsc. Microanal. 18, 745–752. [PubMed: 22832038]

MacDougall DD, Lin Z, Chon NL, Jackman SL, Lin H, Knight JD, Anantharam A, 2018. The high-affinity calcium sensor synaptotagmin-7 serves multiple roles in regulated exocytosis. J. Gen. Physiol. 150, 783–807. [PubMed: 29794152]

Machtens JP, Kortzak D, Lansche C, Leinenweber A, Kilian P, Begemann B, Zachariae U, Ewers D, de Groot BL, Briones R, Fahlke C, 2015. Mechanisms of anion conduction by coupled glutamate transporters. Cell 160, 542–553. [PubMed: 25635461]

Mercer AJ, Rabl K, Riccardi GE, Brecha NC, Stella SL Jr., Thoreson WB, 2011. Location of release sites and calcium-activated chloride channels relative to calcium channels at the photoreceptor ribbon synapse. J. Neurophysiol. 105, 321–335. [PubMed: 21084687]

Miura H, Quadros RM, Gurumurthy CB, Ohtsuka M, 2018. Easi-CRISPR for creating knock-in and conditional knockout mouse models using long ssDNA donors. Nat. Protoc. 13, 195–215. [PubMed: 29266098]

Morgans CW, Bayley PR, Oesch NW, Ren G, Akileswaran L, Taylor WR, 2005. Photoreceptor calcium channels: insight from night blindness. Vis. Neurosci. 22, 561–568. [PubMed: 16332266]

Morgans CW, 2001. Localization of the alpha(1F) calcium channel subunit in the rat retina. Invest. Ophthalmol. Vis. Sci. 42, 2414–2418. [PubMed: 11527958]

Moser T, Grabner CP, Schmitz F, 2020. Sensory processing at ribbon synapses in the retina and the cochlea. Physiol. Rev. 100, 103–144. [PubMed: 31373863]

Nachman-Clewner M, St Jules R, Townes-Anderson E, 1999. L-type calcium channels in the photoreceptor ribbon synapse: localization and role in plasticity. J. Comp. Neurol. 415, 1–16. [PubMed: 10540354]

Nakajima Y, Iwakabe H, Akazawa C, Nawa H, Shigemoto R, Mizuno N, Nakanishi S, 1993. Molecular characterization of a novel retinal metabotropic glutamate receptor mGluR6 with a high agonist selectivity for L-2-amino-4-phosphonobutyrate. J. Biol. Chem. 268, 11868–11873. [PubMed: 8389366]

Otis TS, Jahr CE, 1998. Anion currents and predicted glutamate flux through a neuronal glutamate transporter. J. Neurosci. 18, 7099–7110. [PubMed: 9736633]

Pasquale R, Umino Y, Solessio E, 2020. Rod photoreceptors signal fast changes in daylight levels using a cx36-independent retinal pathway in mouse. J. Neurosci. 40, 796–810. [PubMed: 31776212]

Quadros RM, Miura H, Harms DW, Akatsuka H, Sato T, Aida T, Redder R, Richardson GP, Inagaki Y, Sakai D, Buckley SM, Seshacharyulu P, Batra SK, Behlke MA, Zeiner SA, Jacobi AM, Izu Y, Thoreson WB, Urness LD, Mansour SL, Ohtsuka M, Gurumurthy CB, 2017. Easi-CRISPR: a robust method for one-step generation of mice carrying conditional and insertion alleles using long ssDNA donors and CRISPR ribonucleoproteins. Genome Biol. 18, 92. [PubMed: 28511701]

Rabl K, Cadetti L, Thoreson WB, 2005. Kinetics of exocytosis is faster in cones than in rods. J. Neurosci. 25, 4633–4640. [PubMed: 15872111]

Rao TC, Santana Rodriguez Z, Bradberry MM, Ranski AH, Dahl PJ, Schmidtke MW, Jenkins PM, Axelrod D, Chapman ER, Giovannucci DR, Anantharam A, 2017. Synaptotagmin isoforms confer distinct activation kinetics and dynamics to chromaffin cell granules. J. Gen. Physiol. 149, 763–780. [PubMed: 28687607]

Rao TC, Passmore DR, Peleman AR, Das M, Chapman ER, Anantharam A, 2014. Distinct fusion properties of synaptotagmin-1 and synaptotagmin-7 bearing dense core granules. Mol. Biol. Cell 25, 2416–2427. [PubMed: 24943843]

Sampath AP, Rieke F, 2004. Selective transmission of single photon responses by saturation at the rod-to-rod bipolar synapse. Neuron 41, 431–443. [PubMed: 14766181]

Schmitz F, Konigstorfer A, Sudhof TC, 2000. RIBEYE, a component of synaptic ribbons: a protein's journey through evolution provides insight into synaptic ribbon function. Neuron 28, 857–872. [PubMed: 11163272]

Schnapf JL, Copenhagen DR, 1982. Differences in the kinetics of rod and cone synaptic transmission. Nature 296, 862–864. [PubMed: 6280070]

Schneggenburger R, Rosenmund C, 2015. Molecular mechanisms governing Ca(2+) regulation of evoked and spontaneous release. Nat. Neurosci. 18, 935–941. [PubMed: 26108721]

Schneider N, Cordeiro S, Machtens JP, Braams S, Rauen T, Fahlke C, 2014. Functional properties of the retinal glutamate transporters GLT-1c and EAAT5. J. Biol. Chem. 289, 1815–1824. [PubMed: 24307171]

Smith BJ, Tremblay F, Cote PD, 2013. Voltage-gated sodium channels contribute to the b-wave of the rodent electroretinogram by mediating input to rod bipolar cell GABA(c) receptors. Exp. Eye Res. 116, 279–290. [PubMed: 24060343]

Suryanarayanan A, Slaughter MM, 2006. Synaptic transmission mediated by internal calcium stores in rod photoreceptors. J. Neurosci. 26, 1759–1766. [PubMed: 16467524]

Szikra T, Barabas P, Bartoletti TM, Huang W, Akopian A, Thoreson WB, Krizaj D, 2009. Calcium homeostasis and cone signaling are regulated by interactions between calcium stores and plasma membrane ion channels. PLoS One 4, e6723. [PubMed: 19696927]

Szikra T, Cusato K, Thoreson WB, Barabas P, Bartoletti TM, Krizaj D, 2008. Depletion of calcium stores regulates calcium influx and signal transmission in rod photoreceptors. J. Physiol. 586, 4859–4875. [PubMed: 18755743]

Thoreson WB, 2021. Transmission at rod and cone ribbon synapses in the retina. PflugersArch 473, 1469–1491.

tom Dieck S, Altrock WD, Kessels MM, Qualmann B, Regus H, Brauner D, Fejtova A, Bracko O, Gundelfinger ED, Brandstatter JH, 2005. Molecular dissection of the photoreceptor ribbon synapse: physical interaction of Bassoon and RIBEYE is essential for the assembly of the ribbon complex. J. Cell Biol. 168, 825–836. [PubMed: 15728193]

Turecek J, Regehr WG, 2018. Synaptotagmin 7 mediates both facilitation and asynchronous release at granule cell synapses. J. Neurosci. 38, 3240–3251. [PubMed: 29593071]

Veruki ML, Morkve SH, Hartveit E, 2006. Activation of a presynaptic glutamate transporter regulates synaptic transmission through electrical signaling. Nat. Neurosci. 9, 1388–1396. [PubMed: 17041592]

Vevea JD, Kusick GF, Courtney KC, Chen E, Watanabe S, Chapman ER, 2021. Synaptotagmin 7 is targeted to the axonal plasma membrane through gamma-secretase processing to promote synaptic vesicle docking in mouse hippocampal neurons. Elife 10, e67261. [PubMed: 34543184]

Wachtmeister L, 1998. Oscillatory potentials in the retina: what do they reveal. Prog. Retin. Eye Res. 17, 485–521. [PubMed: 9777648]

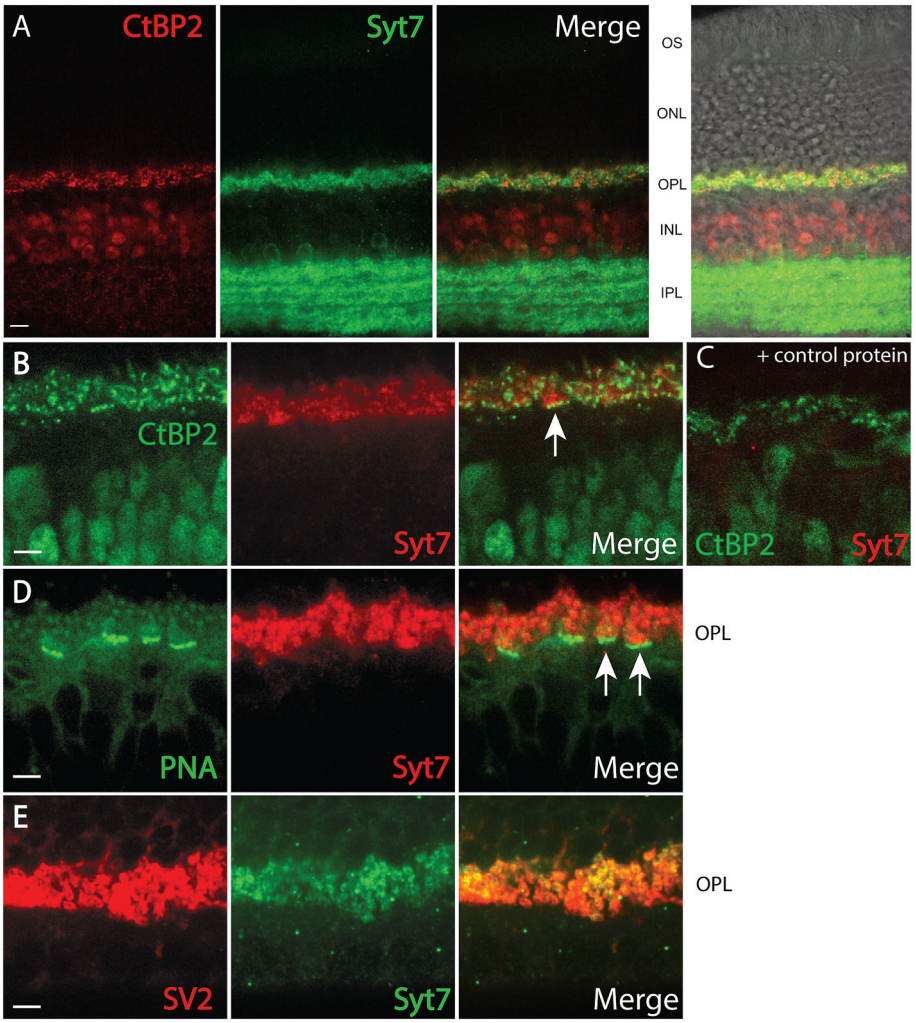

Fig. 1.

Immunohistochemical results showed the presence of Syt7 in the outer plexiform layer (OPL) and inner plexiform layer (IPL). A) Ribeye protein in synaptic ribbons was labeled with an antibody to CtBP2 (Santa Cruz) and stained with a rhodamine-conjugated secondary antibody (Thermo Fisher, red, left). Syt7 was labeled using the Synaptic Systems antibody along with a FITC-conjugated secondary antibody (BD Biosciences; green, middle). Merged images show overlap of Syt7 with CtBP2 labeling in the OPL and IPL (right). Merged image is overlaid on a bright-field image of the same slice in the panel at the far right. Along with OPL and IPL, layers shown in that image are photoreceptor outer segments (OS), outer nuclear layer (ONL) and inner nuclear layer (INL). The INL is stained by the CtBP2 antibody due to the presence of a shorter, non-Ribeye variant of CtBP2. B. Magnified view of the OPL showing CtBP2 (BD Biosciences) labeled with a FITC-conjugated secondary antibody (BD Biosciences, green) and Syt7 (Synaptic Systems) labeled with rhodamine-conjugated antibody (Thermo Fisher, red). The arrow points to a cone terminal with multiple ribbons in the merged image. C. Another retinal section labeled for CtBP2 (BD Biosciences, green) and Syt7 (Synaptic Systems, red). This image shows that labeling for Syt7 was abolished by pre-incubation with the fusion peptide used for immunization to create the

Synaptic Systems antibody. D. OPL labeled with FITC-conjugated peanut agglutinin (PNA; green) and Syt7 antibody (Synaptic Systems) labeled with a rhodamine secondary (Thermo Fisher, red). PNA labels the base of cone terminals and the arrows in the merged image point to two cone terminals that are also labeled by the Syt7 antibody. E. OPL labeled with antibodies to the vesicle protein, SV2 (DSHB, green) and Syt7 (Synaptic Systems, red). Single confocal sections. Scale bar in A: 10 μm. Scale bar in B–E: 5 μm. (For interpretation of the references to colour in this figure legend, the reader is referred to the Web version of this article.)

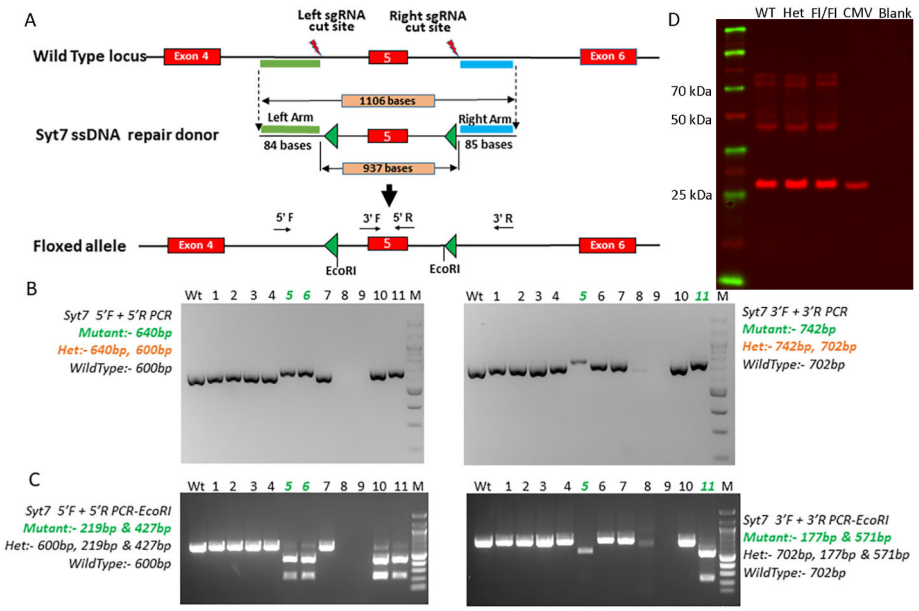

Fig. 2.

A: Schematics showing the wild type locus and floxing design for targeting exon 5 of Syt7. The floxed allele was generated using the Easi-CRISPR method (Quadros et al., 2017) that uses long single-stranded DNA as the repair donor template. The lengths of ssDNA, homology arms, and the distance between the two *LoxP* sites are shown. B: Genotyping of F0 offspring. Two PCRs, one each for the two *LoxP* sites (5′ *LoxP* PCR, 5′ F + 5′ R primers; 3′ *LoxP* PCR, 3′ F + 3′ R primers) were used to identify targeted mice. The expected sizes of PCR amplicons (wild type or floxed) are shown at the left and right of the gel images. C: PCR-RFLP (Restriction Fragment Length Polymorphism) using EcoRI digestion was used to further confirm the correctly targeted mice. The expected sizes of RFLP fragments (wild type or floxed) are shown at the left and right of the gel images. Agarose gel images of the two sets of genotyping assays (B and C) showed that animals #5 and #11 contained correctly targeted floxed alleles. Animal #6 contained only 5′ *LoxP* site and animals #8 and 9 may have had deletion of the targeted region. Founders 5 and 11 were bred to establish floxed mice colonies. D: Western blot of whole brain protein shows deletion of a band at the predicted molecular weight of ~45 kDa in a homozygous $Syt7^{KO}$ mouse ($Syt7^{flfl}$/CMVCre; labeled “CMV”) with no change evident in a heterozygous $Syt7^{fl}$/CMVCre (“Het”) or Cre-negative $Syt7^{fl/fl}$ (“Fl/Fl”) mouse compared to a control C57Bl6J mouse (“WT”).

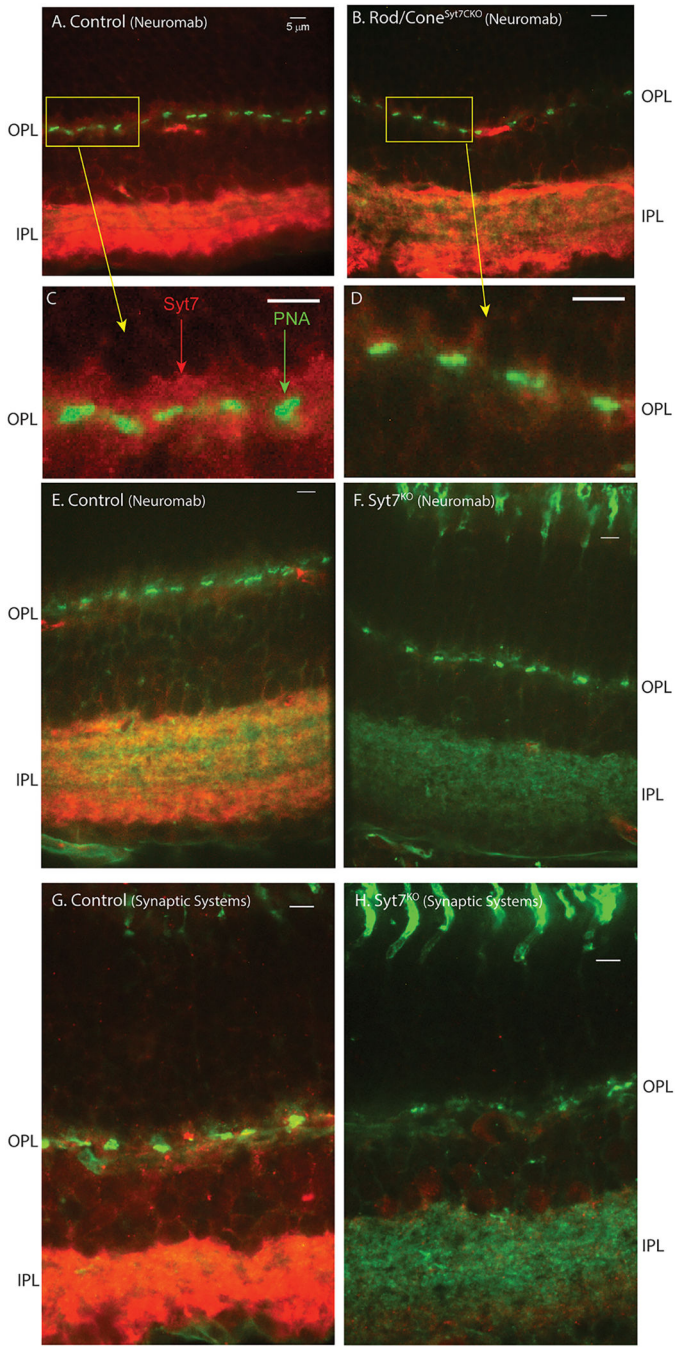

Fig. 3.

Syt7 labeling in the OPL and IPL of mouse retina. A: Control C57Bl6 mouse retina labeled with Neuromab antibodies to Syt7 and visualized with a rhodamine-conjugated secondary antibody (Thermo Fisher, red). These sections were co-stained with FITC-PNA (Sigma, green) to label cone terminals. FITC-PNA also stains cone inner segments and the IPL. B: Labeling with Syt7 antibodies in a Rod/Cone^{Syt7CKO} mouse retina. Other than labeling of a blood vessel by the secondary antibody, staining in the OPL was largely eliminated by deletion of Syt7 from rods and cones, although bright labeling remained in the IPL

as expected. Labeling for Syt7 in the OPL and its absence in Rod/Cone^{Syt7CKO} mouse retina can be seen more readily in the magnified image in panels C and D, respectively. Brightness was increased in the red channel equally in panels C and D to enhance the visibility of Syt7 labeling. E: Control retina labeled with Neuromab Syt7 antibodies and FITC-PNA. F: Labeling for Syt7 was abolished from both the OPL and IPL in a Syt7^{KO} mouse (CMV^{Syt7KO}). G: Retina of a control C57Bl6 mouse labeled with Synaptic Systems Syt7 antibody along with FITC-PNA to label cone terminals. H: Labeling for Syt7 with the Synaptic Systems antibody was also abolished from both the OPL and IPL in a Syt7^{KO} mouse (CMV^{Syt7KO}). Single confocal sections. Scale bars: 5 μm. (For interpretation of the references to colour in this figure legend, the reader is referred to the Web version of this article.)

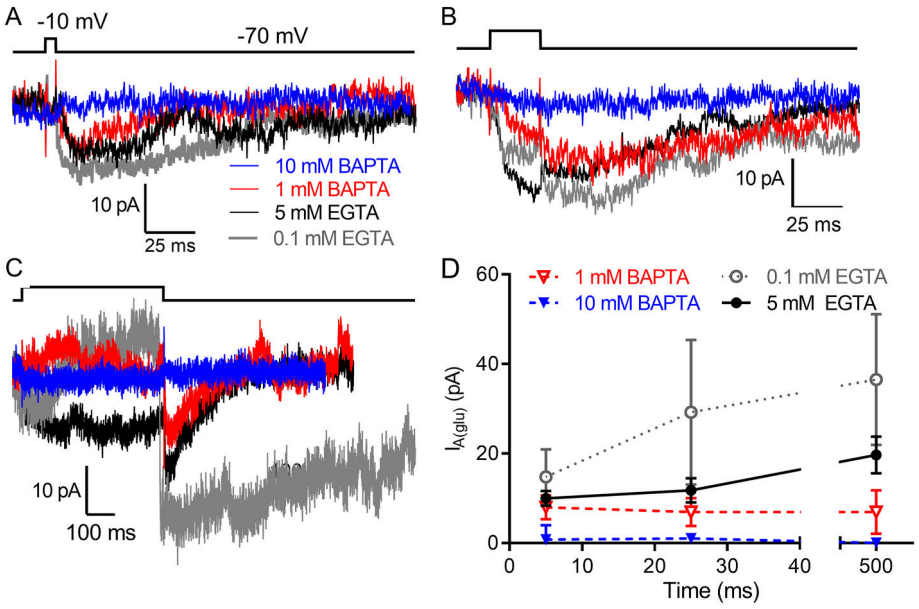

Fig. 4.

Effects of intracellular Ca^{2+} buffering on $I_{A\ (Glu)}$ in rods from control C57Bl6 and Cre^{-} mice evoked with strong depolarizing steps (−70 to −10 mV). A: Representative $I_{A(Glu)}$ evoked by 5 (A), 25 (B) and 500 (C) ms steps. Overlaid traces show currents evoked with different intracellular Ca^{2+} buffers introduced into rods through the patch whole cell recording pipette (0.1 mM EGTA, gray; 5 mM EGTA, black; 1 mM BAPTA, red; 10 mM BAPTA, blue). The stimulus trace is shown at the top of each panel. D. Summary data showing changes in $I_{A(Glu)}$ amplitude with the various buffers. Buffering with 1 mM BAPTA (open red triangles, n = 17 rods, 6 mice) reduced $I_{A\ (Glu)}$ evoked by 500 ms step significantly compared to control conditions (filled black circles, 5 mM EGTA, n = 56, $p < 0.0001$, *t*-test corrected for multiple comparisons). 0.1 mM EGTA (open gray circles, n = 10 rods, 7 mice) significantly enhanced responses evoked by 25 ms ($p < 0.001$) and 500 ms ($p < 0.001$) steps. Responses evoked by strong depolarizing steps were abolished by 10 mM BAPTA (filled blue triangles, n = 3 rods) compared to 5 mM EGTA with all step durations ($p = 0.002$, 5 ms; $p = 0.008$, 25 ms; $p < 0.0001$; 500 ms). Error bars show 95% confidence intervals. (For interpretation of the references to colour in this figure legend, the reader is referred to the Web version of this article.)

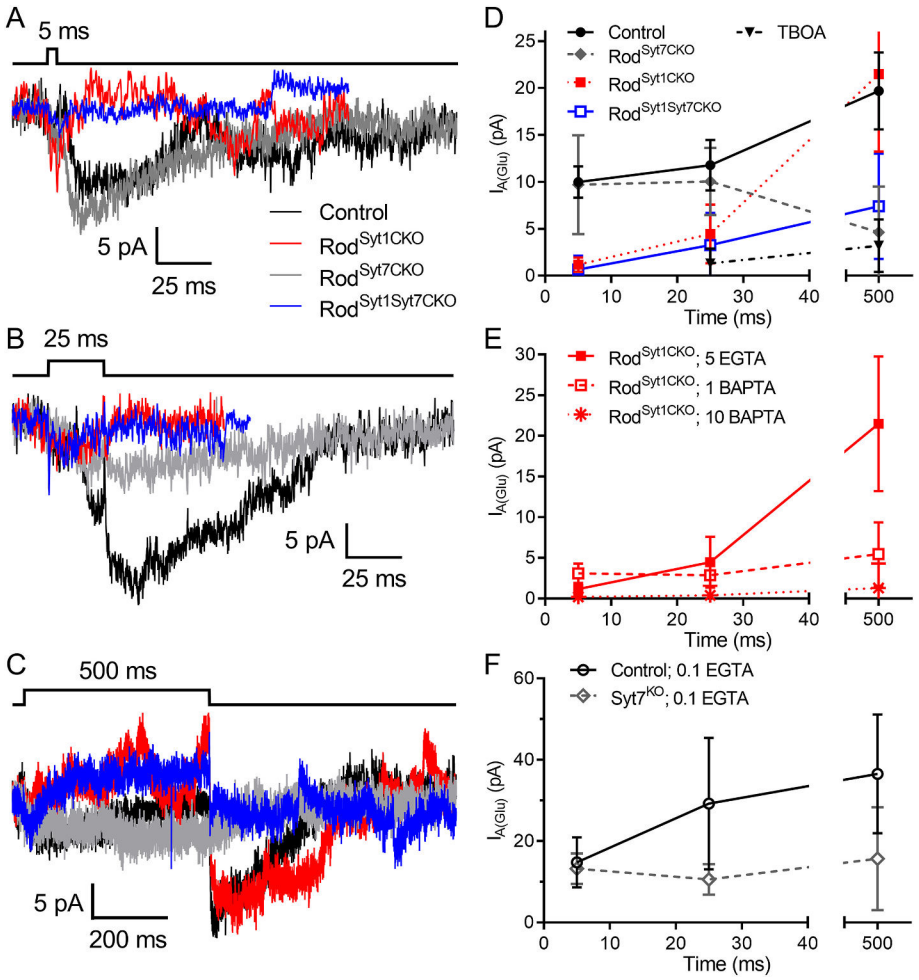

Fig. 5.

$I_{A(Glu)}$ recordings from rods show that eliminating Syt1 diminishes fast release whereas eliminating Syt7 diminishes slower components of depolarization-evoked glutamate release. The traces in A, B and C show overlaid examples of $I_{A(Glu)}$ recorded from rods in four different mouse lines: control (black traces), $Rod^{Syt1CKO}$ (red traces), $Rod^{Syt7CKO}$ (gray traces), and $Rod^{Syt1/Syt7CKO}$ (blue traces) with 5 mM EGTA as the Ca^{2+} buffer. D. Plot of $I_{A(Glu)}$ amplitude as a function of test step duration (−70 to −10 mV) in recordings from control (filled black circles, n = 42–56), control + TBOA (0.3 mM, filled black triangles, n = 8 rods, 3 mice), $Rod^{Syt1CKO}$ (filled red squares, n = 30 rods, 11 mice), $Rod^{Syt7CKO}$ (filled gray diamonds, n = 7 rods, 5 mice), and $Rod^{Syt1/Syt7CKO}$ mice (open blue squares, n = 8 rods, 3 mice). Responses of $Rod^{Syt7CKO}$ and $Rod^{Syt1/Syt7CKO}$ mice were both significantly different (Tukey's multiple comparisons test) from control (P = 0.0024 and 0.021, respectively) and $Rod^{Syt1CKO}$ (P = 0.0004 and 0.0049, respectively) mice at 500 ms. $Rod^{Syt1CKO}$ rods were significantly different from control at 5 ms and 25 ms (p = 0.0013). Control data were replotted from Fig. 4D. E. $I_{A(Glu)}$ vs. step duration in rods from $Rod^{Syt1CKO}$ mice recorded with pipette solutions containing 1 mM BAPTA (open red squares, n = 14 rods) and 10 mM BAPTA (red asterisks, n = 5 rods). Data from $Rod^{Syt1CKO}$ mice recorded with 5 mM EGTA (filled red squares) are replotted from D for comparison.

Responses were depressed at 500 ms by both 1 (p = 0.0003) and 10 mM BAPTA (p = 0.0002). F. $I_{A\ (Glu)}$ vs. step duration in rods from $Syt7^{KO}$ mice (CMV^{Syt7KO}) recorded with 0.1 mM EGTA in the pipette solution (open gray diamonds, n = 13–17 rods). Data from control rods recorded with 0.1 mM EGTA are replotted from Fig. 4 for comparison (open black circles). Error bars show 95% confidence intervals. (For interpretation of the references to colour in this figure legend, the reader is referred to the Web version of this article.)

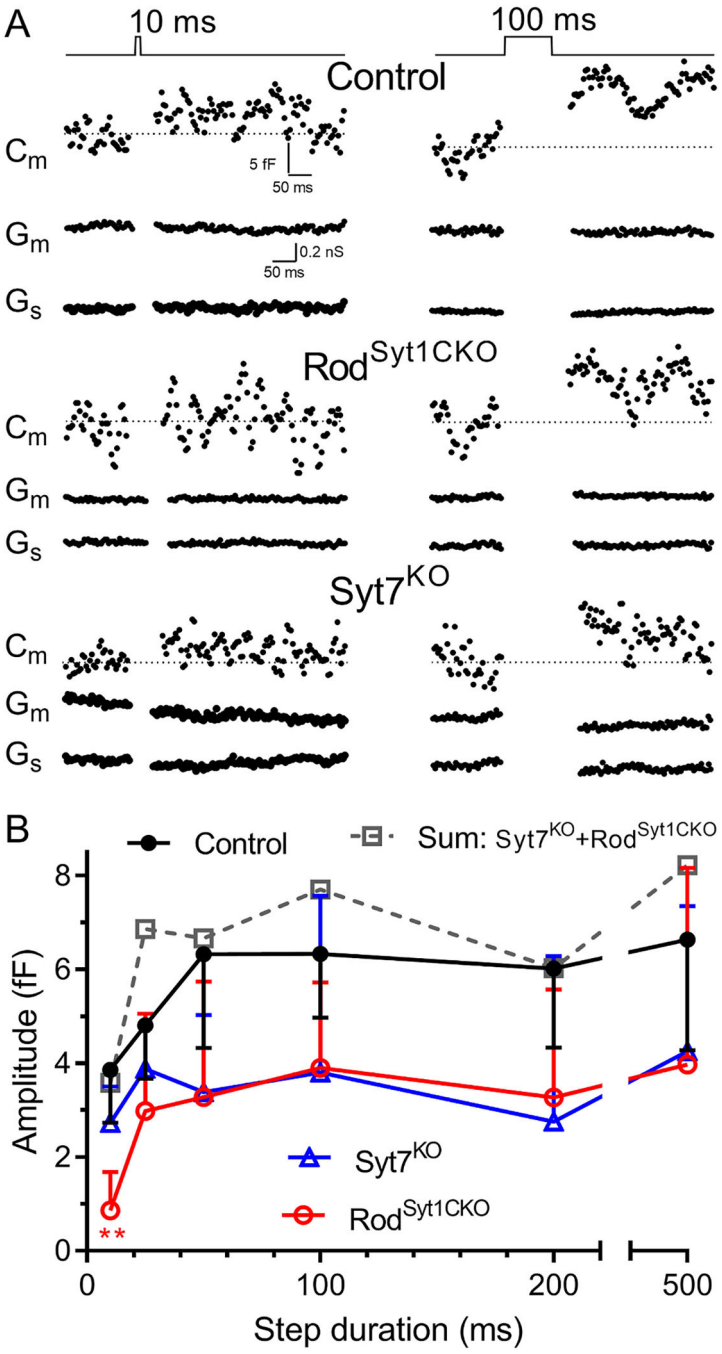

Fig. 6.

Exocytotic capacitance responses in rods showed that eliminating Syt1 reduces fast release whereas eliminating Syt7 reduces slower release. A. Examples of membrane capacitance (C_m), membrane conductance (G_m), and access conductance (G_s) from control, $Rod^{Syt1CKO}$, and $Syt7^{KO}$ rods. Test stimuli were 10 and 100 ms steps from −70 to −10 mV. Each stimulus pair was from the same rod. B. Exocytotic capacitance increases plotted as a function of test step duration. Control (filled black circles): 10 ms, n = 24 rods; 25 ms, n = 19; 50 ms, n = 16; 100 ms, n = 21; 200 ms, n = 15; 500 ms, n = 15. $Rod^{Syt1CKO}$ (open red circles): 10

ms, n = 12 rods; 25 ms, n = 11; 50 ms, n = 9; 100 ms, n = 11; 200 ms, n = 7; 500 ms, n = 6. $Syt7^{KO}$ (open blue triangles): 10 ms, n = 9 rods; 25 ms, n = 8; 50 ms, n = 6; 100 ms, n = 5; 200 ms, n = 4; 500 ms, n = 8. Rod responses in $Rod^{Syt1CKO}$ and $Syt7^{KO}$ mice were significantly smaller than control responses (control vs. $Rod^{Syt1CKO}$, $P < 0.0001$; control vs. $Syt7^{KO}$, $P = 0.0043$, Dunnett's multiple comparisons test). Error bars show 95% confidence intervals. **: p = 0.00419, *t*-test corrected for multiple comparisons with False Discovery Rate approach). (For interpretation of the references to colour in this figure legend, the reader is referred to the Web version of this article.)

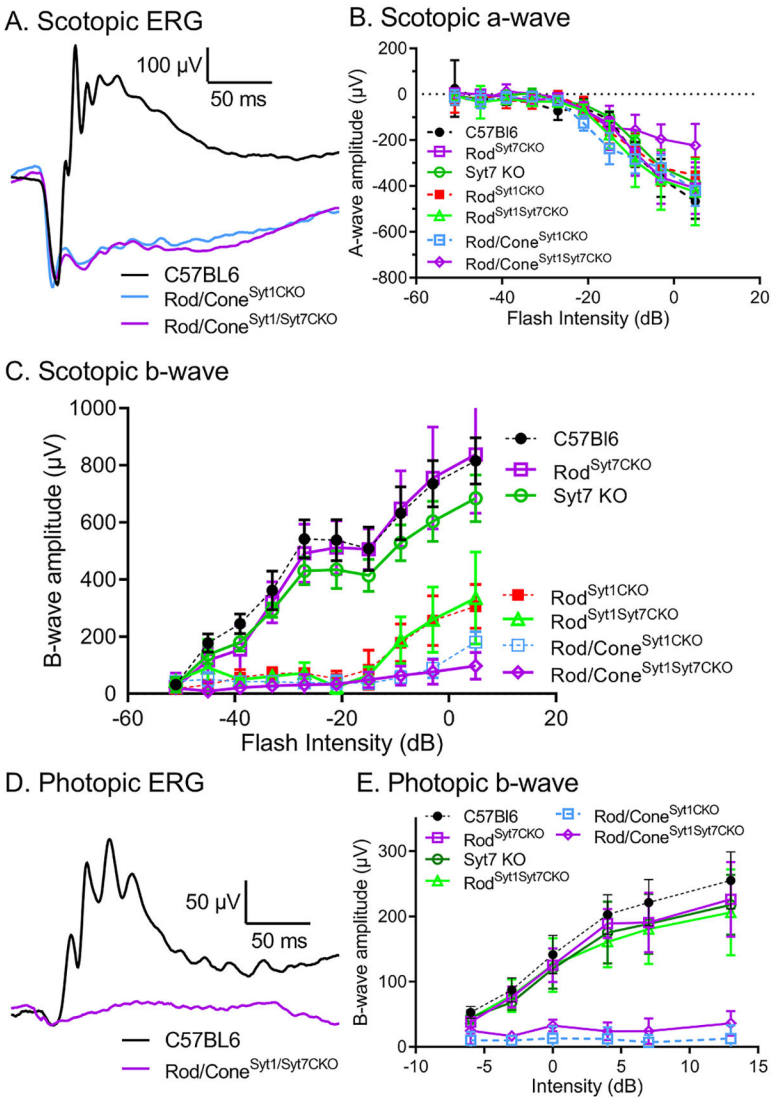

Fig. 7.

Minimal effects of Syt7 on the ERG. A: Example ERG waveforms evoked by a 20 ms high intensity (−3 dB) flash applied to dark-adapted mouse retina. Responses are from C57Bl6, Rod/Cone^{Syt1CKO} and Rod/Cone^{Syt1Syt7CKO} mice. B: Scotopic ERG a-wave amplitudes in C57Bl6 (filled black circles, n = 6), Syt7 KO (open green circles, n = 7), Rod^{Syt7CKO} (open purple squares, n = 4), Rod^{Syt1CKO} (filled red squares, n = 7), Rod^{Syt1Syt7CKO} (open green triangles, n = 5), Rod/Cone^{Syt1CKO} (open pale blue squares, n = 7), and Rod/Cone^{Syt1Syt7CKO} (open purple diamonds, n = 6) mice. C: B-wave amplitudes evoked under scotopic conditions as a function of flash intensity in C57Bl6 (n = 6 mice), Syt7 KO (n = 5), Rod^{Syt7CKO} (n = 4), Rod^{Syt1CKO} (n = 7), Rod^{Syt1Syt7CKO} (n = 5), Rod/Cone^{Syt1CKO} (n = 7) and Rod/Cone^{Syt1Syt7CKO} (n = 6) mice. Scotopic b-waves were significantly reduced relative to control in Syt7 KO (P = 0.0008), Rod^{Syt1CKO} (P = 0.0010), Rod^{Syt1Syt7CKO} (P = 0.0019), Rod/Cone^{Syt1CKO} (P = 0.0023) and Rod/Cone^{Syt1Syt7CKO} (P = 0.0016) mice. D: Example of photopic ERGs evoked by a bright flash (+13 dB) in C57Bl6 and Rod/Cone^{Syt1Syt7CKO} mice. E: Photopic b-wave amplitudes in C57Bl6 (n = 6), Syt7 KO (n = 5), Rod^{Syt7CKO} (n =

4) mice, $Rod^{Syt1Syt7CKO}$ (n = 5), $Rod/Cone^{Syt1CKO}$ (n = 7) and $Rod/Cone^{Syt1Syt7CKO}$ (n = 6) mice. Photopic b-waves from $Rod/Cone^{Syt1CKO}$ (p = 0.023) and $Rod/Cone^{Syt1Syt7CKO}$ mice (p = 0.032, Dunnett's multiple comparisons test) both differed significantly from control. Error bars show ±S.D. (For interpretation of the references to colour in this figure legend, the reader is referred to the Web version of this article.)

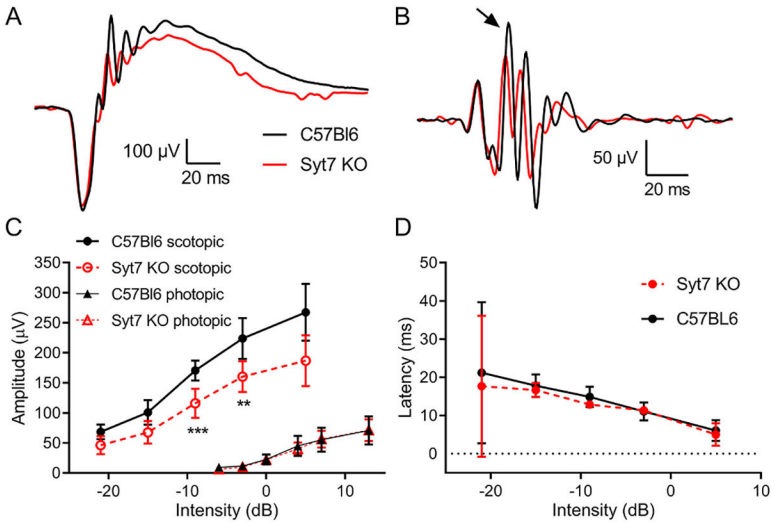

Fig. 8.

Effects of Syt7 elimination from the whole retina on ERG oscillatory potentials. A: Example waveforms of ERG responses to a bright flash (5 dB) applied under scotopic conditions in control and Syt7 KO mice. B: Oscillatory potentials extracted from the same pair of responses by bandpass filtering to remove frequencies below 70 Hz and above 280 Hz. C: Oscillatory potential amplitude as a function of flash intensity. Circles show scotopic responses and triangles show photopic responses. Filled black symbols show responses of control C57Bl6 mice (n = 7 mice) whereas open red symbols show responses of Syt7 KO mice (n = 7). Under scotopic conditions, the two samples differed significantly (mixed effects analysis, $P < 0.0001$) and the reduction in OPs in Syt7 KO achieved statistical significance at two intensities (−9 dB, $P = 0.00059$; −3 dB, $P = 0.00325$; unpaired *t*-test corrected for multiple comparisons, Holm-Sidak method). D: The latency to the largest positive peak (indicated by the arrow in B) did not differ between control and Syt7 KO mice. **: $P < 0.01$; ***$P < 0.001$. Error bars show ±S.D. (For interpretation of the references to colour in this figure legend, the reader is referred to the Web version of this article.)

Table 1

Key resources table.

Reagent type	Designation	Source or reference	Identifiers	Additional information
Mouse strain	Rho-iCre	Jackson Lab.	RRID:IMSR_JAX:015850	Rod-specific iCre
Mouse strain	HRGP-Cre	Le et al., 2004Jackson Lab.	Tg(OPN1LW-cre)4Yzl/J	Cone-specific Cre
Mouse strain	$Syt1^{fl/fl}$	Quadros et al., 2017Jackson Lab.	MMRRC:065805-MU	Floxed Syt1 gene
Mouse strain	$Syt7^{fl/fl}$	UNMC Mouse Genome Engineering Core	NA	Floxed Syt7 gene
Mouse strain	CMV^{cre}	Jackson Lab.	RRID:IMSR_JAX:006054	Global Cre expression
Reagent	FITC-conjugated peanut agglutinin	Sigma	L7381	0.5 mg/ml
Reagent	Donkey Serum	Jackson Immunoresearch	RRID:AB_11000165	
Reagent	Goat Serum	Life Technologies	16210064	
Antibody	Mouse anti-Syt7 supernatan	NeuroMab/Antibodies Inc.	RRID: AB_2337254	1:10
Antibody	Polyclonal rabbit anti-Syt7	Synaptic Systems	105–173	1:400–1:500
Antibody	Donkey anti-rabbit (Alexa Fluor 568)	Thermo Fisher	A10042; RRID: AB_2534017	1:200–1:500
Antibody	Donkey anti-goat (AlexFluor488)	Thermo Fisher	A11055; RRID:AB_253673	1:200
Antibody	Goat anti-mouse(rhodamine)	Thermo Fisher	R6393; RRID:AB_2556550	1:200–1:500
Antibody	Goat anti-mouse (FITC)	BD Biosciences	554001; RRID:AB_395197	1:200
Antibody	Goat anti-CtBP2	Santa Cruz	sc-5966; RRID:AB 2086774	1:150
Antibody	Mouse anti-CtBP2	BD Biosciences	612044; RRID:AB_399431	1:2000
Antibody	Mouse anti-SV2	DSHB	Concentrate	1:1000